Int. J. Heat Mass Transfer. Vol. 34, No. 7, pp. 1605–1616, 1991
Printed in Great Britain

0017–9310/91 $3.00 + 0.00

Effects of V-shaped rib arrays on turbulent heat transfer and friction of fully developed flow in a square channel

S. C. LAU, R. T. KUKREJA and R. D. McMILLIN
Department of Mechanical Engineering, Texas A&M University, College Station, TX 77843-3123, U.S.A.

(*Received* 30 *April* 1990 *and in final form* 6 *August* 1990)

Abstract—This study examines turbulent heat transfer and friction characteristics of fully developed flow of air in a square channel in which two opposite walls are roughened with aligned arrays of V-shaped ribs. The rib-roughened channel models the internal cooling passages in modern gas turbine airfoils. The angles-of-attack of the V-shaped rib arrays are 45°, 60°, 90° (same as 90° full ribs), 120°, and 135°. The 60° V-shaped ribs with $p/e = 10$ have the highest ribbed wall heat transfer and smooth wall heat transfer for a given air flow rate, and the highest channel heat transfer per unit pumping power. They are recommended for internal turbine airfoil cooling, replacing 45° or 60° full ribs.

INTRODUCTION

RESEARCHERS have modeled internal cooling passages in modern gas turbine airfoils as straight and/or multi-pass rectangular channels that had two opposite ribbed walls and two smooth walls. Prior work such as Burggraf [1], Han [2], and Han *et al.* [3] examined the effects of varying the rib angle-of-attack, the rib pitch-to-height ratio, and the rib height-to-channel hydraulic diameter ratio on the heat transfer in such a straight, square, rib-roughened channel. These studies concluded that parallel 60° full ribs enhanced the channel heat transfer the most and caused the highest pressure drop. Parallel full ribs with $\alpha = 45°$ had the highest cooling rate for a given pumping power.

Experiments were conducted to study the effects of replacing the 90° full ribs on two opposite walls of a square channel with discrete ribs on the turbulent heat transfer and friction for fully developed flow of air in the square channel [4]. The discrete ribs were five equal-length segments of the 90° full ribs staggered in alternate rows of three and two ribs. In the angled discrete rib cases, the ribs on opposite walls were turned an angle equal to α either in the same direction (parallel arrays on opposite walls) or in opposite directions (crossed arrays) with respect to the main flow. Results showed that, for the flow Reynolds number between 10 000 and 80 000, the ribbed wall heat transfer in the 90° discrete rib case was higher than that in the 90° full rib case. Parallel discrete ribs with $\alpha = 60°$, 45°, and 30° enhanced the ribbed wall heat transfer and the overall heat transfer more than the 90° discrete ribs and had better thermal performances than 90° discrete ribs. Crossed angled discrete ribs performed poorly and were not recommended.

The thermal performances of angled discrete ribs (five equal-length segments of the angled full ribs cut at an angle equal to α) and corresponding angled full ribs for thermally fully developed flow in a square channel were compared in ref. [5]. The discrete ribs were staggered in alternate rows of three and two ribs along oblique lines at α with respect to the main flow. Parallel angled discrete ribs had higher ribbed wall heat transfer, lower smooth wall heat transfer, and lower channel pressure drop than parallel angled full ribs. Parallel 60° discrete ribs had the highest ribbed wall heat transfer and crossed 30° discrete ribs caused the lowest pressure drop. Parallel discrete ribs with $\alpha = 30°$ had the highest thermal performance, but their performance was only slightly better than those of the parallel discrete ribs with $\alpha = 45°$ and 60°.

This investigation examines the heat transfer augmentation caused by V-shaped ribs on two opposite walls of a square channel. Attention is focused on the effects of varying the rib angle-of-attack on the heat transfer and pressure drop for thermally fully developed flow of air in the square channel. The V-shaped rib results are compared with published data for corresponding angled full ribs.

Air flow in a square channel with aligned, parallel arrays of V-shaped ribs on two opposite walls and two smooth walls differ from that in a square channel that has two opposite walls roughened with 90° full ribs or angled full ribs. Near the walls with the V-shaped ribs, the flow separates on the top edges of the ribs and is guided along the two straight segments of the ribs either toward the two smooth walls (when $\alpha < 90°$) or toward the ribbed wall centerlines away from the two smooth walls (when $\alpha > 90°$). It is postulated that, as a result of geometric symmetry of the channel, the secondary flows wash adjacent ribbed and smooth walls, and generate four counter-rotating vortexes that force the cooler air in the middle of the channel toward the centerlines of the ribbed walls or the smooth walls, depending on whether the angle-of-attack of the V-shaped ribs is smaller than or larger

NOMENCLATURE

a coefficient in roughness functions
b exponent in roughness functions
c_p specific heat of air at average bulk temperature [J kg^{-1} K^{-1}]
D hydraulic diameter of square channel [m]
dP/dx streamwise pressure gradient in fully developed region in channel [(N m^{-2}) m^{-1}]
e height of ribs [m]
e^+ roughness Reynolds number, equation (5)
$\bar{f}$ friction factor for square channel with two opposite ribbed walls and two smooth walls, equation (3)
f_{ss} friction factor for square channel with four smooth walls
$G(e^+, Pr)$ heat transfer roughness function, equation (7)
$\bar{G}(e^+, Pr)$ average heat transfer roughness function, equation (8)
$\dot{m}$ rate of mass flow of air [kg s^{-1}]
p rib pitch [m]
P local static pressure [N m^{-2}]
$\dot{q}''_r$ net heat flux on ribbed walls [W m^{-2}]
$\dot{q}''_s$ net heat flux on smooth walls [W m^{-2}]
$R(e^+)$ roughness function, equation (6)
Re_D Reynolds number based on channel hydraulic diameter, equation (4)
$\overline{St}$ average Stanton number, the average of St_r and St_s
St_r Stanton number for ribbed walls in square channel with two opposite ribbed walls and two smooth walls, equation (1)
St_s Stanton number for smooth walls in square channel with two opposite ribbed walls and two smooth walls, equation (2)
St_{ss} Stanton number for square channel with four smooth walls
$(T_{wr} - T_b)$ average ribbed wall/bulk temperature difference in fully developed region in channel [K]
$(T_{ws} - T_b)$ average smooth wall/bulk temperature difference in fully developed region in channel [K]
$\bar{u}$ average air velocity [m s^{-1}]
x streamwise coordinate [m].

Greek symbols
α rib angle-of-attack [deg]
μ dynamic viscosity of air at average bulk temperature [N s m^{-2}]
ρ density of air at average bulk temperature [kg m^{-3}]
τ_w average wall shear stress [N m^{-2}]

Subscripts
r ribbed walls in square channel with two opposite ribbed walls and two smooth walls
s smooth walls in square channel with two opposite ribbed walls and two smooth walls
ss square channel with four smooth walls
90 square channel with 90° full ribs on two opposite ribbed walls and two smooth walls.

than 90°. The possibilities of two counter-rotating vortexes and one vortex in the flows through a square channel with parallel and crossed angled full ribs, respectively, were discussed in ref. [5]. Since parallel full ribs have consistently higher thermal performances than corresponding crossed full ribs, the additional counter-rotating vortexes in the parallel V-shaped rib cases may cause better mixing in the flow, and may increase the heat transfer and thermal performances over those of parallel angled ribs.

EXPERIMENTAL APPARATUS AND PROCEDURE

The open air flow loop is similar to that used in two earlier studies [4, 5]. It consists of two centrifugal blowers connected in parallel (one blower for low flow rate tests), two gate valves, a calibrated orifice flow meter, a flow straightener, an entrance section, and the test section (Fig. 1). The test section is a straight, square channel made of aluminum. It is 1.52 m long and has a cross section of 7.62 by 7.62 cm. Each wall of the test section is heated uniformly with an electric heater, the power input to each heater being controlled with a variable transformer. A thin gasket minimizes heat conduction between adjacent channel walls and prevents air leakage. The test section, along

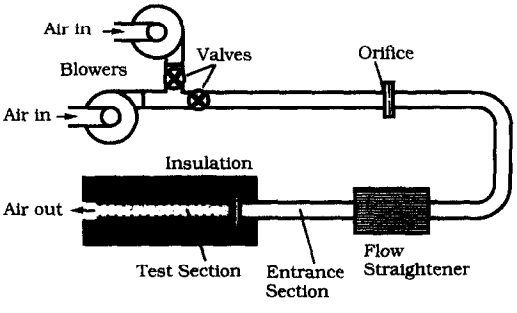

FIG. 1. Schematic of test apparatus.

with the downstream half of the acrylic entrance section, is heavily insulated with fiberglass felt.

The interior surfaces of two opposite walls of the test channel are roughened with aligned arrays of V-shaped ribs. The interior surfaces of the other two walls are smooth. Each V-shaped rib has two straight angled-cut segments. These segments are cut from 4.76 by 4.76 mm square brass bars. Therefore, the rib height-to-channel hydraulic diameter ratio, e/D, in this study is 0.0625. The ribs are attached to the channel walls with silicone rubber adhesive at intervals of either 4.76 or 9.52 cm (that is, the rib pitch-to-height ratio is either 10 or 20) with the first ribs located at $x = 0$.

Five angles-of-attack of the V-shaped ribs are studied: 45°, 60°, 90° (same as transverse full ribs), 120°, and 135° (Fig. 2). Table 1 gives the configurations of the V-shaped ribs in the various cases in this study. In all cases except case 8, the rib arrays on the opposite walls are aligned and parallel. In case 8, the angles-of-attack of the ribs on the two opposite walls are 60° and 120°, respectively. That is, the V-shaped rib arrays on the two opposite walls are aligned but crossed. In cases 1a, 5a, and 6a, the rib pitch-to-height ratio, p/e, is equal to 20, while in all other cases, $p/e = 10$. The V-shaped rib results of this study are compared with those in corresponding full rib cases (full rib results of cases 1, 2, and 3 were previously reported in ref. [5]).

Since each V-shaped rib consists of two straight segments, 128 rib segments are needed in all cases with $p/e = 10$; 64 are needed in cases with $p/e = 20$. Individual rib segments are cut at an angle equal to α with a slitting saw on a milling machine. After the rib segments are installed onto the channel walls, the clearance between the end surfaces of the V-shaped ribs and the adjacent smooth walls is 0.76 mm, which is 1% of the width of the channel walls.

Table 1. Rib configurations

Case	Rib array†	α (deg)	p/e
1‡	Full	90	10
1a	Full	90	20
2‡	Full	45	10
3‡	Full	60	10
4	V-Shaped	45	10
5	V-Shaped	60	10
5a	V-Shaped	60	20
6	V-Shaped	120	10
6a	V-Shaped	120	20
7	V-Shaped	135	10
8	V-Shaped/crossed	60/120	10

† Rib arrays on opposite walls are aligned and are parallel except in case 8.

‡ Reported in ref. [5].

Thirty-nine 30-gage copper–constantan thermocouples are installed along the axial centerlines of the ribbed walls and the smooth walls to determine the streamwise wall temperature distributions. The first thermocouple station is located at 2.5 times the rib height from the channel entrance. Twelve other temperature measurement stations are located at 30 rib-height intervals. Nine other thermocouples along the axial centerlines of the ribbed walls and the smooth walls check the streamwise temperature variation between adjacent primary measurement stations in the thermally fully developed region. Six additional thermocouples at other off-center locations on the ribbed walls check the spanwise variation of the wall temperature.

Two thermocouples measure the inlet air temperature and four thermocouples the exit air temperature. Three pressure taps are installed along the axial centerline of one of the smooth walls at 0.46, 0.91, and 1.37 m, respectively, from the test section entrance to determine the streamwise pressure drop.

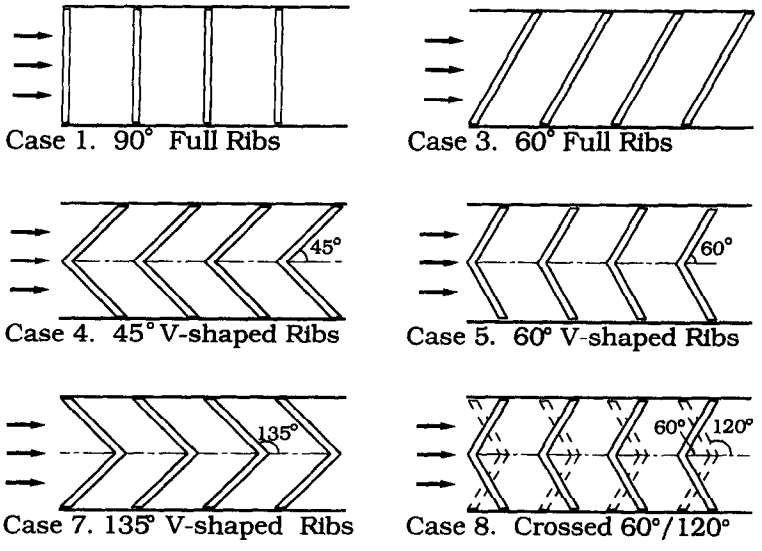

FIG. 2. Typical rib configurations.

A data logger reads the thermocouple output. A micromanometer measures the local pressure drops in the test channel. U-Tube and inclined manometers measure the pressure drop across the orifice and the gage pressure upstream of the orifice. Two TRMS multimeters measure the voltage drop across each heater and the current through each heater, respectively.

To prepare the test apparatus for a set of experiments, the ribs used in the previous set of experiments are removed and the interior surfaces of the test section are cleaned thoroughly with an adhesive solvent. The ribs for the experiments are then installed. Extreme care is taken to position the rib segments accurately and to ensure good metal-to-metal contact at the rib–wall interfaces. After the test section is reassembled, the blower is switched on to allow air to flow through the test channel and a solution of soap and water is used to check for air leakage. The preparation procedure generally lasts 8–10 h.

To initiate an experiment, air at a predetermined mass flow rate is allowed to flow through the test channel. Power is then supplied to the heaters to maintain the wall temperatures near the exit at about 15°C above the exit air temperature. To minimize conduction between adjacent walls, more heat is supplied to the two ribbed walls than to the two smooth walls so that, at any axial location, the wall temperatures on the two ribbed walls and the two smooth walls are about the same.

Steady state is attained in $1\frac{1}{2}$–2 h. The heater voltages and currents along with all temperatures and pressures are then recorded. The maximum variations of some of the readings are also recorded for the uncertainty analysis of the results. The barometric pressure is read at the beginning and the end of a test run.

For each rib configuration, seven to eight experiments are conducted at air flow rates corresponding to the flow Reynolds numbers (based on the channel hydraulic diameter) between 10 000 and 60 000. Four smooth-channel (no-rib) calibration experiments are also conducted. The values of the overall Nusselt number are within 6% of the corresponding values calculated with the modified Dittus–Boelter equation. The values of the overall friction factor are consistently higher than those calculated with the modified Karman–Prandtl equation, but by no more than 5%. The modified Dittus–Boelter and Karman–Prandtl equations can be found in ref. [4].

In separate no-flow experiments, a correlation between the rate of heat loss through the fiberglass insulation and the average wall temperature is obtained [4]. The correlation estimates the rates of heat loss through the insulation at the various wall temperature measurement stations during a test run.

DATA REDUCTION

The reduction of the experimental data follows the procedure given in ref. [4]. The ribbed wall and smooth wall Stanton numbers are calculated, respectively, from

$$St_r = \dot{q}_r'' D^2/[\dot{m}c_p(\overline{T_{wr}} - \overline{T_b})] \quad (1)$$

and

$$St_s = \dot{q}_s'' D^2/[\dot{m}c_p(T_{ws} - \overline{T_b})] \quad (2)$$

where the average wall/bulk temperature differences are the averages of the differences between the measured wall temperatures and the calculated air bulk temperatures (at the corresponding streamwise locations) over a section of the test channel between the primary measurement stations at $x/D = 7.66$ and 15.16, where the flow is considered thermally fully developed. Experimental data show that there is no measurable spanwise temperature variation in each wall, the streamwise wall temperature distribution in each wall is linear in this section of the channel, and the wall temperatures and the bulk temperatures between $x/D = 7.66$ and 15.16 fall on parallel lines in plots of temperatures vs x/D.

In equation (1), the heat flux on the ribbed walls is the rate of net heat transfer from the ribbed walls to the flowing air divided by the projected heat transfer area (not including the increased rib surface area). The rate of net heat transfer from each channel wall to the flowing air is the sum of the rates of net heat transfer from 'imaginary segments' of the wall in the thermally fully developed region. These wall segments (equivalent to control volumes in finite difference analysis) have interfaces between adjacent temperature measurement stations. For each segment, the rate of net heat transfer is the power input to the portion of the heater over that segment minus the rate of heat loss through the insulation plus the net rate of heat gain as a result of streamwise heat conduction between the segment and adjacent wall segments.

The rate of heat loss through the insulation is determined both (a) numerically assuming a uniform temperature (equal to the measured temperature) over the segment, one-dimensional heat conduction, and an equivalent thickness of the insulation, and (b) with the measured temperature and the heat loss–wall temperature correlation from the no-flow experiments. There is no significant difference between the two heat loss values. Streamwise heat conduction in the channel wall is estimated from the measured wall temperatures assuming one-dimensional heat conduction and a linear streamwise wall temperature distribution between consecutive measurement stations.

The distribution of the bulk temperature is evaluated from an energy balance with the sum of the rates of net heat transfer from adjacent segments of all four walls to the air, the air mass flow rate, and the inlet bulk temperature. For 90% of the test runs, the calculated exit bulk temperature is within 1.0°C of the measured average exit air temperature.

The average Stanton number, $\overline{St}$, is the average of the Stanton numbers for the ribbed walls and the

smooth walls. The friction factor and the Reynolds number are defined respectively as

$$\bar{f} = \tau_w/[(1/2)\rho\bar{u}^2]$$
$$= [(-dP/dx)D/4]/[(1/2)\rho\bar{u}^2]$$
$$= [(-dP/dx)D^5/[2(\dot{m}^2/\rho)] \quad (3)$$

$$Re_D = \rho\bar{u}D/\mu = \dot{m}/(D\mu). \quad (4)$$

In equations (1)–(4), all properties of the flowing air are evaluated at the average bulk temperature.

The maximum uncertainties of the values of the Reynolds number, the Stanton numbers, and the friction factor are estimated to be ± 2.9, ± 5.8, and $\pm 10.9\%$ respectively [6]. The uncertainties of $\bar{f}$ are relatively large since the pressure drop in the test section is quite small when the flow rate is low.

The friction factor and the Stanton numbers are normalized with their corresponding values for thermally fully developed turbulent flow through a square channel that has two opposite walls roughened with 90° full ribs and two smooth walls, $\bar{f}_{90}$, $St_{r,90}$, $St_{s,90}$, and $\overline{St}_{90}$ (case 1).

The roughness Reynolds number, e^+, the roughness function, $R(e^+)$, the heat transfer roughness function, $G(e^+, Pr)$, and the average heat transfer roughness function, $\bar{G}(e^+, Pr)$, are determined with the following equations [4]:

$$e^+ = (e/D)\, Re_D[(2\bar{f}-f_{ss})/2]^{0.5} \quad (5)$$

$$R(e^+) = [(2\bar{f}-f_{ss})/2]^{-0.5}+2.5\ln[2(e/D)]+2.5 \quad (6)$$

$$G(e^+, Pr) = [(2\bar{f}-f_{ss})/2]^{0.5}/St_r+2.5\ln[2(e/D)]+2.5 \quad (7)$$

$$\bar{G}(e^+, Pr) = [(2\bar{f}-f_{ss})/2]^{0.5}/\overline{St}+2.5\ln[2(e/D)]+2.5. \quad (8)$$

The roughness functions are for the prediction of the Stanton numbers and friction factors in cases with different values of e/D.

PRESENTATION OF RESULTS

By curve fitting least-squares straight lines through experimental data for $p/e = 10$ given in ref. [5], the ribbed wall Stanton number, the smooth wall Stanton number, the average Stanton number, and the friction factor in the 90°, 45°, and 60° full rib cases are obtained, respectively, as power functions of the flow Reynolds number as follows:

Case 1: full ribs with $\alpha = 90°$

$$St_r = 0.1464\,(Re_D)^{-0.2745}$$
$$St_s = 0.08994\,(Re_D)^{-0.2817}$$
$$\overline{St} = 0.1184\,(Re_D)^{-0.2774}$$

and

$$\bar{f} = 0.07155\,(Re_D)^{-0.07636} \quad (9a)$$

Case 2: full ribs with $\alpha = 45°$

$$St_r = 0.4772\,(Re_D)^{-0.3742}$$
$$St_s = 0.1023\,(Re_D)^{-0.2711}$$
$$\overline{St} = 0.2583\,(Re_D)^{-0.3350}$$

and

$$\bar{f} = 0.1267\,(Re_D)^{-0.1330} \quad (9b)$$

Case 3: full ribs with $\alpha = 60°$

$$St_r = 0.3859\,(Re_D)^{-0.3389}$$
$$St_s = 0.07073\,(Re_D)^{-0.2332}$$
$$\overline{St} = 0.2015\,(Re_D)^{-0.3008}$$

and

$$\bar{f} = 0.07394\,(Re_D)^{-0.04494}. \quad (9c)$$

The ribbed wall Stanton number, the smooth wall Stanton number, the average Stanton number, and the friction factor in the V-shaped rib cases with $p/e = 10$ are then normalized with those in the 90° full rib case. The normalized ribbed wall Stanton number and smooth wall Stanton number, $St_r/St_{r,90}$ and $St_s/St_{s,90}$, are plotted as functions of the rib angle-of-attack for $Re_D \cong 10\,000$, 15 000, 30 000, 40 000, and 60 000 in Fig. 3. Similarly, the variations of the normalized average Stanton number and friction factor, $\overline{St}/\overline{St}_{90}$ and $\bar{f}/\bar{f}_{90}$, with the rib angle-of-attack and the Reynolds number are shown in Fig. 4. In the two figures, $St_r/St_{r,90}$, $St_s/St_{s,90}$, $\overline{St}/\overline{St}_{90}$, and $\bar{f}/\bar{f}_{90}$ for the 45° and 60° full rib cases from equations (9b) and (9c) are included for comparison. The values of the normalized Stanton numbers and friction factor give the improvement in heat transfer and the penalty in higher pressure drop when 90° full ribs are replaced with V-shaped ribs and angled full ribs.

Rib angle effect on heat transfer

All parallel arrays of V-shaped ribs with $\alpha = 45°$, 60°, 120°, and 135° enhance more heat from the ribbed walls and the smooth walls than 90° full ribs. Over the range of Reynolds number studied, the values of St_r in the 45° and 60° V-shaped rib cases are 38–46% and 47–66% higher than those in the 90° full rib case, respectively. The values of St_r in the 120° and 135° V-shaped rib cases are 39–48% and 26–32% higher than those in the 90° full rib case.

The 60° V-shaped ribs have higher ribbed wall heat transfer than the 45° V-shaped ribs; the 120° V-shaped ribs have higher ribbed wall heat transfer than the 135° V-shaped ribs. Since the 45° and 60° V-shaped ribs have higher ribbed wall heat transfer than the 135° and 120° V-shaped ribs, respectively, reversing the 45° and 60° V-shaped ribs lowers the ribbed wall heat transfer.

The 60° V-shaped ribs enhance the smooth wall heat transfer the most—about 60% over the 90° full

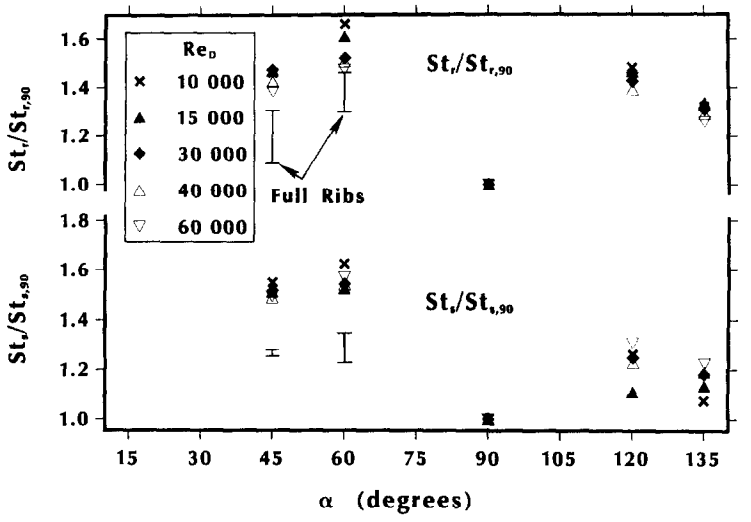

FIG. 3. $St_r/St_{r,90}$ and $St_s/St_{s,90}$ as functions of α, V-shaped ribs with $p/e = 10$.

ribs, followed in order by the 45°, 120°, and 135° V-shaped ribs. Reversing the 45° and 60° V-shaped ribs also lowers the smooth wall heat transfer.

Comparing corresponding 45° and 60° V-shaped ribs with angled full ribs, the V-shaped ribs have much higher heat transfer from both the ribbed walls and the smooth walls than the angled full ribs. Replacing the 45° full ribs with the 135° V-shaped ribs improves the ribbed wall heat transfer slightly but lowers the smooth wall heat transfer. The 120° V-shaped ribs have higher ribbed wall heat transfer than the 60° full ribs; the smooth wall heat transfer in the two cases, however, are comparable.

Rib angle effect on pressure drop

Although the V-shaped ribs have higher ribbed wall and smooth wall heat transfer than the 90° full ribs, they also cause higher pressure drop (Fig. 4). The 45° and 60° V-shaped ribs increase the pressure drop 55–72% and 68–79% over the 90° full ribs, respectively. The reverse V-shaped ribs (α = 120° and 135°) have even higher pressure drop—the values of $\bar{f}/\bar{f}_{90}$ range from 1.84 to 2.13 and from 1.58 to 1.86, respectively. The values of $\bar{f}$ in the 45° full rib case are about the same as those in the 90° full rib case (that is, $\bar{f}/\bar{f}_{90} \cong 1.00$) and those in the 60° full rib case are only about 40% higher than the values of $\bar{f}_{90}$.

Rib angle effect on thermal performance

Figure 5 compares the thermal performances of the V-shaped ribs with those of the angled full ribs. The ratios $[(St_r/St_{r,90})/(\bar{f}/\bar{f}_{90})^{1/3}]$ and $[(\overline{St}/\overline{St}_{90})/(\bar{f}/\bar{f}_{90})^{1/3}]$ for all cases with $p/e = 10$ are plotted vs the rib angle-of-attack for $Re_D \cong 10\,000$, 15 000, 30 000, 40 000, and 60 000. The 60° V-shaped ribs have the highest thermal performance. Their performance is followed, in order,

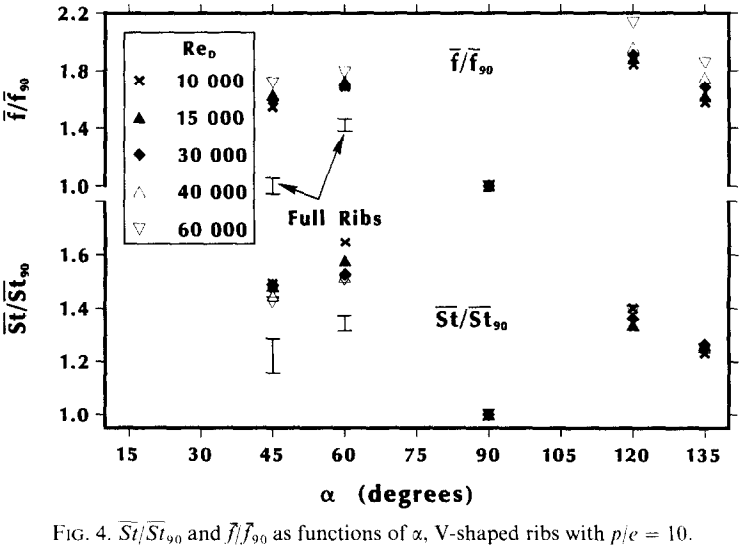

FIG. 4. $\overline{St}/\overline{St}_{90}$ and $\bar{f}/\bar{f}_{90}$ as functions of α, V-shaped ribs with $p/e = 10$.

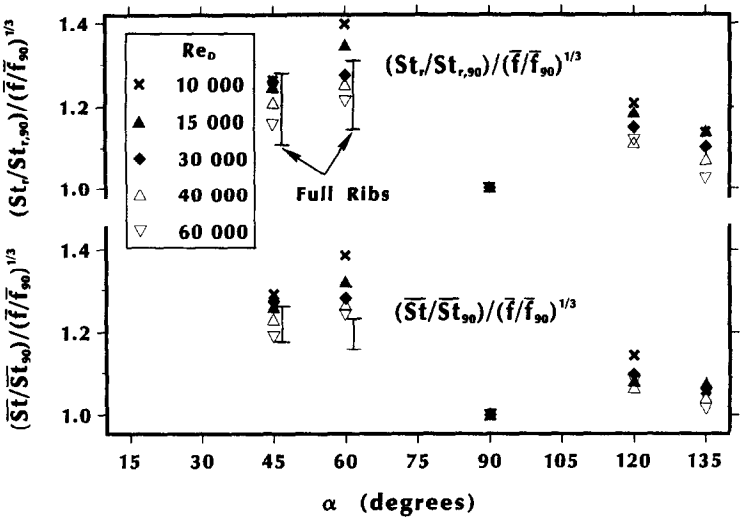

FIG. 5. Thermal performances of V-shaped ribs, $[(St_r/St_{r,90})/(\bar{f}/\bar{f}_{90})^{1/3}]$ and $[(\overline{St}/\overline{St}_{90})/(\bar{f}/\bar{f}_{90})^{1/3}]$ as functions of α, $p/e = 10$.

by those of the 45° V-shaped ribs, the 120° V-shaped ribs, and the 135° V-shaped ribs. The overall thermal performances of the reverse V-shaped ribs are only slightly higher than that of the 90° full ribs with almost all values of $[(\overline{St}/\overline{St}_{90})/(\bar{f}/\bar{f}_{90})^{1/3}] < 1.10$.

The 60° V-shaped ribs outperform the 60° full ribs, for $10\,000 < Re_D < 60\,000$. The 60° V-shaped ribs have values of $[(St_r/St_{r,90})/(\bar{f}/\bar{f}_{90})^{1/3}]$ and $[(\overline{St}/\overline{St}_{90})/(\bar{f}/\bar{f}_{90})^{1/3}]$ ranging from 1.21 to 1.40 and from 1.24 to 1.39, respectively; the 60° full ribs have corresponding values ranging from 1.14 to 1.31 and from 1.16 to 1.23.

The 45° V-shaped ribs and the 45° full ribs have similar thermal performances. For $10\,000 < Re_D < 60\,000$, the values of $[(St_r/St_{r,90})/(\bar{f}/\bar{f}_{90})^{1/3}]$ and $[(\overline{St}/\overline{St}_{90})/(\bar{f}/\bar{f}_{90})^{1/3}]$ in the two cases differ by no more than 4%.

Reynolds number effect

Figures 6–8 show that the ratios $St_r/St_{r,90}$, $St_s/St_{s,90}$, $\overline{St}/\overline{St}_{90}$, $\bar{f}/\bar{f}_{90}$, $[(St_r/St_{r,90})/(\bar{f}/\bar{f}_{90})^{1/3}]$, and $[(\overline{St}/\overline{St}_{90})/(\bar{f}/\bar{f}_{90})^{1/3}]$ for the various V-shaped rib cases with $p/e = 10$ are power functions of the Reynolds number. For comparison purposes, lines representing the power functions for the 45° and 60° full ribs are also shown.

The 60° V-shaped ribs have the highest ribbed wall heat transfer, smooth wall heat transfer, and thermal performance. The 45° and 60° V-shaped ribs have higher ribbed wall heat transfer, smooth wall heat transfer, and pressure drop than corresponding angled full ribs. The reverse V-shaped ribs ($\alpha = 120°$ and 135°) have high pressure drops and low thermal performances.

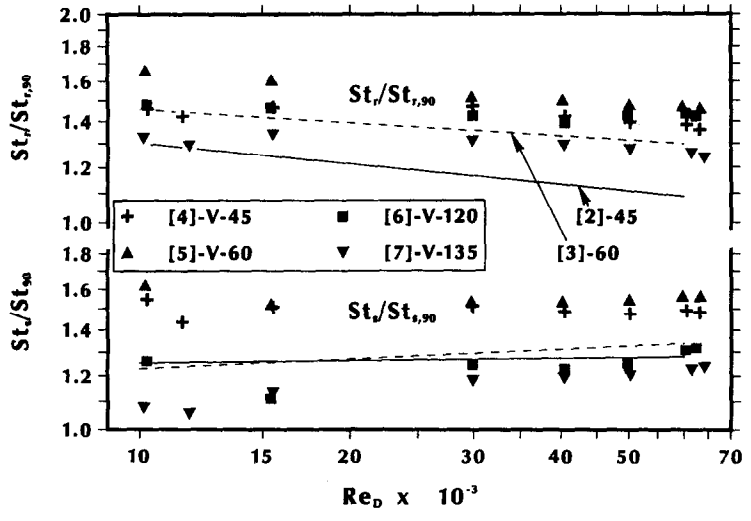

FIG. 6. $St_r/St_{r,90}$ and $St_s/St_{s,90}$ as functions of Re_D, V-shaped ribs with $p/e = 10$.

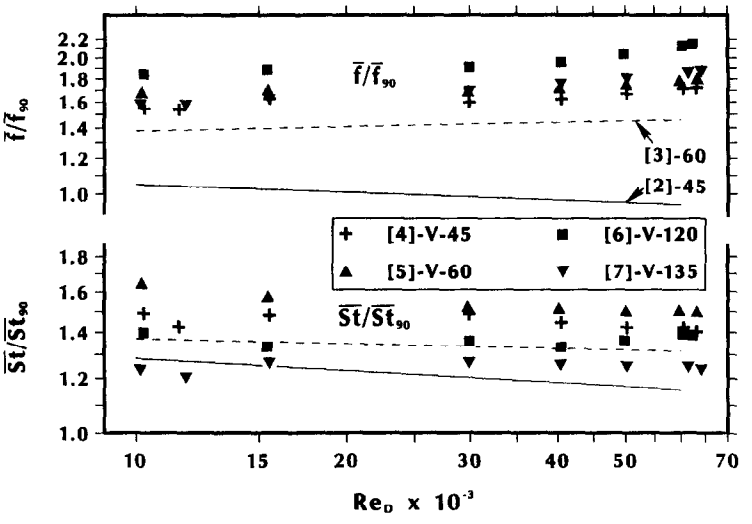

FIG. 7. $\bar{St}/\bar{St}_{90}$ and $\bar{f}/\bar{f}_{90}$ as functions of Re_D, V-shaped ribs with $p/e = 10$.

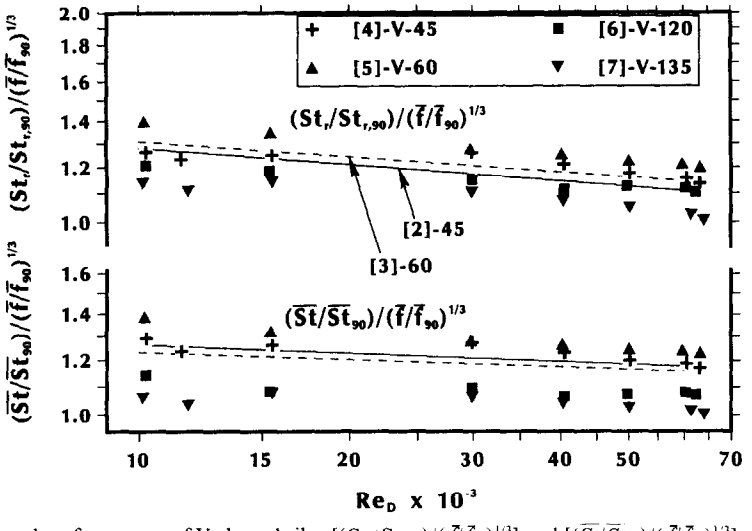

FIG. 8. Thermal performances of V-shaped ribs, $[(St_r/St_{r,90})/(\bar{f}/\bar{f}_{90})^{1/3}]$ and $[(\bar{St}/\bar{St}_{90})/(\bar{f}/\bar{f}_{90})^{1/3}]$ as functions of Re_D, $p/e = 10$.

Parallel and crossed ribs

Figures 9 and 10 illustrate the effects of crossing the V-shaped arrays (on opposite walls) on the channel heat transfer and pressure drop. The heat transfer on the wall with the 60° V-shaped ribs in case 8 (the crossed rib case) is slightly lower than the ribbed wall heat transfer in case 5 (with parallel 60° V-shaped ribs on opposite walls); the heat transfer on the wall with 120° V-shaped ribs in case 8 is lower than the ribbed wall heat transfer in case 6 (with parallel 120° V-shaped ribs on opposite walls). The smooth wall heat transfer in the crossed 60°/120° V-shaped rib case is comparable to that in the 120° V-shaped rib case and is much lower than that in the 60° V-shaped rib case. The overall heat transfer and the pressure drop in case 8 are lower than those in both cases 5 and 6. It can be shown that the thermal performance of the crossed 60°/120° V-shaped ribs is only slightly better than that of the 120° V-shaped ribs and is much worse that that of the 60° V-shaped ribs.

Rib pitch effect

The Stanton numbers, friction factors, and thermal performances of V-shaped ribs with $p/e = 20$ (cases 1a, 5a, and 6a) are compared with those of V-shaped ribs with $p/e = 10$ (cases 1, 5, and 6). In Figs. 11–13, the Stanton numbers and friction factor are normalized with those for thermally fully developed flow through a square channel with four smooth walls (using the modified Karman–Prandtl and Dittus–Boelter equations) and are plotted vs the flow Reynolds number. Doubling the rib pitch-to-height ratio

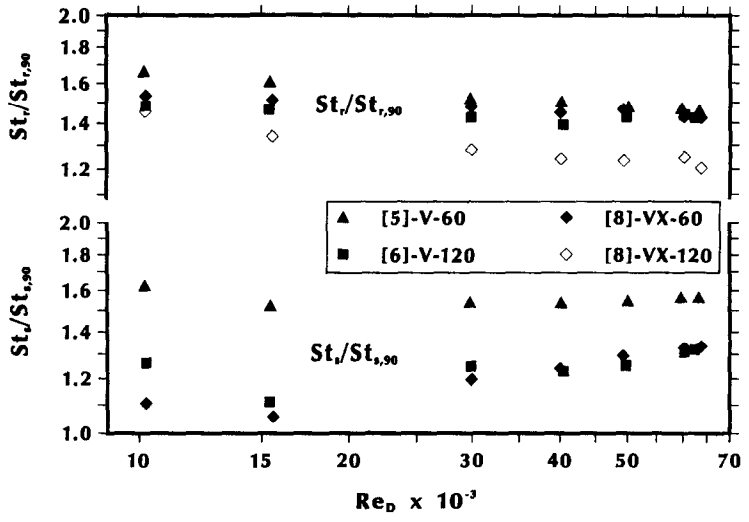

FIG. 9. Comparison of $St_r/St_{r,90}$ and $St_s/St_{s,90}$ of parallel and crossed V-shaped ribs with $p/e = 10$.

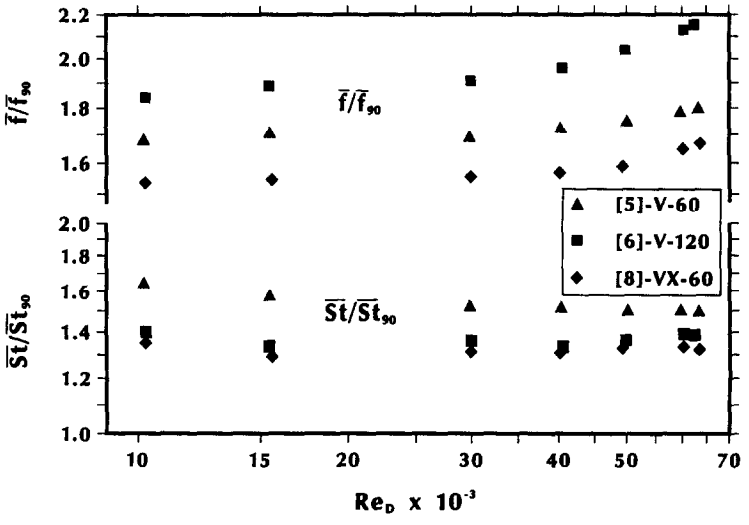

FIG. 10. Comparison of $\overline{St}/\overline{St}_{90}$ and $\bar{f}/\bar{f}_{90}$ of parallel and crossed V-shaped ribs with $p/e = 10$.

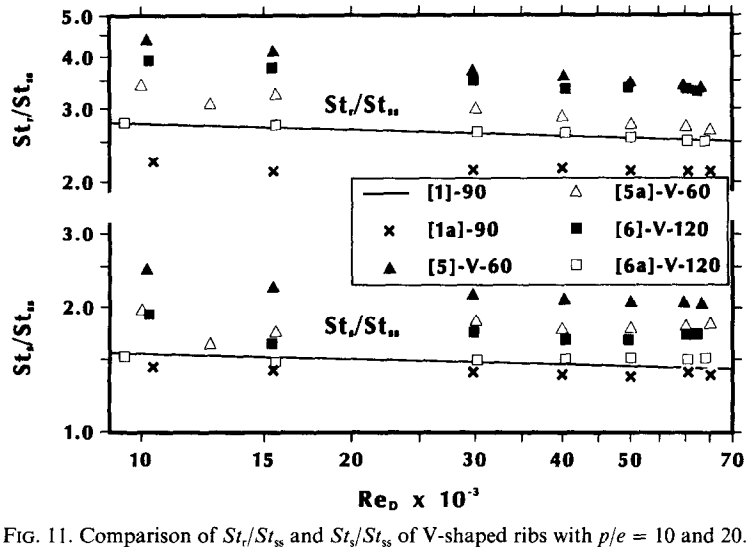

FIG. 11. Comparison of St_r/St_{ss} and St_s/St_{ss} of V-shaped ribs with $p/e = 10$ and 20.

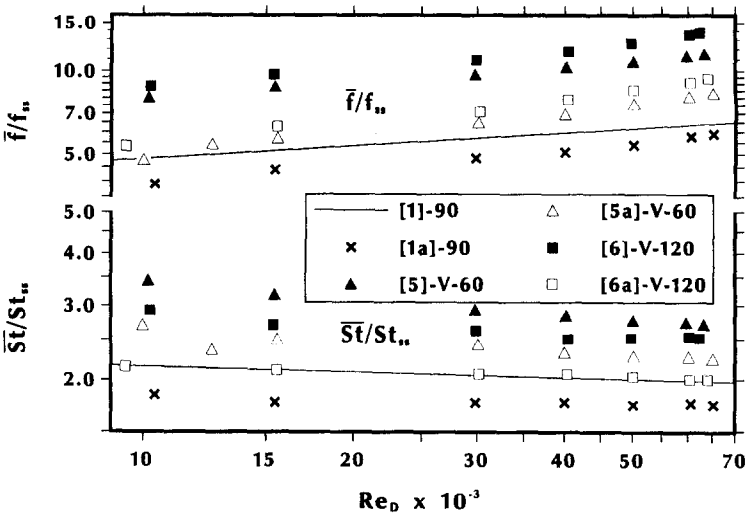

FIG. 12. Comparison of $\overline{St}/St_{ss}$ and $\bar{f}/f_{ss}$ of V-shaped ribs with $p/e = 10$ and 20.

from 10 to 20 lowers the ribbed wall heat transfer, the smooth wall heat transfer, the friction factor, and the thermal performance. For $p/e = 20$, both the 60° and 120° V-shaped ribs have higher values of St_r/St_{ss}, St_s/St_{ss}, $\overline{St}/St_{ss}$, $\bar{f}/f_{ss}$, $[(St_r/St_{ss})/(\bar{f}/f_{ss})^{1/3}]$, and $[(\overline{St}/St_{ss})/(\bar{f}/f_{ss})^{1/3}]$ than 90° full ribs. Again, reversing the 60° V-shaped ribs lowers the channel wall heat transfer, increases the pressure drop, and lowers the thermal performance.

To correlate the experimental data for the prediction of Stanton numbers and friction factor, $R(e^+)$, $G(e^+, Pr)$, and $\bar{G}(e^+, Pr)$, are expressed as power functions of e^+. The coefficients and exponents of the functions are given in Table 2.

CONCLUDING REMARKS

Experiments have been conducted to study the turbulent heat transfer and friction characteristics of fully developed flow of air in a square channel in which two opposite walls are roughened with aligned arrays of V-shaped ribs. The following conclusions are drawn:

(1) The 60° V-shaped ribs with $p/e = 10$ have the highest ribbed wall heat transfer, smooth wall heat transfer, and thermal performance. The 60° V-shaped ribs outperform the 60° full ribs, for $10\,000 < Re_D < 60\,000$. The 60° V-shaped ribs with $p/e = 10$ have values of $[(St_r/St_{r,90})/(\bar{f}/\bar{f}_{90})^{1/3}]$ and

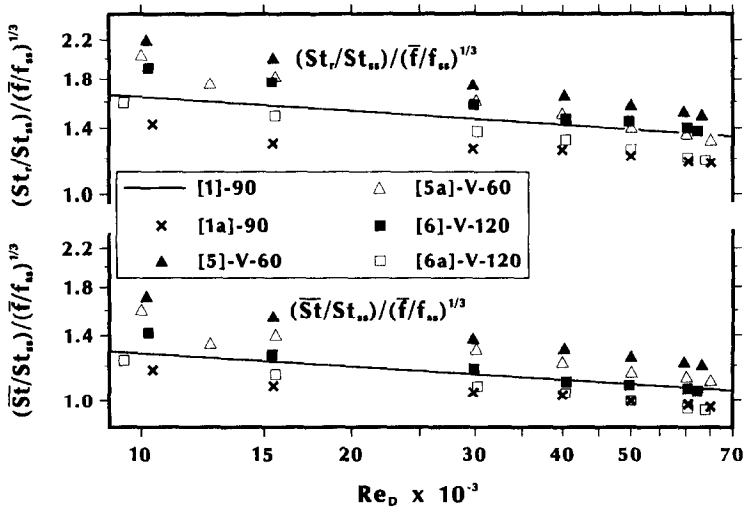

FIG. 13. Comparison of thermal performances of V-shaped ribs with $p/e = 10$ and 20.

Table 2. Coefficients and exponents for the functions $R(e^+)$, $G(e^+, Pr)$, and $\bar{G}(e^+, Pr)$

Case/configuration designation	$R(e^+) = a(e^+)^b$		$G(e^+, Pr) = a(e^+)^b$		$\bar{G}(e^+, Pr) = a(e^+)^b$	
	a	b	a	b	a	b
1a/-90	3.674	−0.0033	4.218	0.257	5.450	0.250
4/-V-45	1.605	0.0015	1.819	0.355	2.656	0.335
5/-V-60	1.232	0.0454	1.299	0.399	2.163	0.360
5a/-V-60	3.687	−0.0571	1.685	0.376	2.719	0.336
6/-V-120	1.537	−0.0228	1.983	0.352	3.460	0.315
6a/-V-120	3.617	−0.0734	2.739	0.324	4.351	0.291
7/-V-135	2.070	−0.0384	1.992	0.362	3.685	0.313

$[(St/St_{90})/(\bar{f}/\bar{f}_{90})^{1/3}]$ ranging from 1.21 to 1.40 and from 1.24 to 1.39, respectively; the 60° full ribs with $p/e = 10$ have corresponding values ranging from 1.14 to 1.31 and from 1.16 to 1.23.

(2) The 45° V-shaped ribs and the 45° full ribs with $p/e = 10$ have similar thermal performances. For $10\,000 < Re_D < 60\,000$, the values of $[(St_r/St_{r,90})/(\bar{f}/\bar{f}_{90})^{1/3}]$ and $[(\overline{St}/\overline{St}_{90})/(\bar{f}/\bar{f}_{90})^{1/3}]$ in the two cases differ by no more than 4%.

(3) The 45° and 60° V-shaped ribs with $p/e = 10$ enhance more heat transfer from both the ribbed walls and the smooth walls, but cause higher pressure drop than corresponding angled full ribs and 90° full ribs. For $10\,000 < Re_D < 60\,000$, the ribbed wall Stanton numbers in the 45° and 60° V-shaped rib cases (with $p/e = 10$) are 38–46% and 47–66% higher than that in the 90° full rib case, respectively; the corresponding pressure drops are 55–72% and 68–79% higher than that in the 90° full rib case.

(4) Reversing the 45° and 60° V-shaped rib arrays lowers the heat transfer from the channel walls and increases the channel pressure drop. The reverse V-shaped ribs ($\alpha = 120°$ and 135°) have high pressure drops and low thermal performances.

(5) Crossing the 60° V-shaped rib arrays on the opposite walls improves neither the heat transfer from the channel walls nor the overall thermal performance.

(6) Doubling the rib pitch-to-height ratio from 10 to 20 lowers the ribbed wall heat transfer, the smooth wall heat transfer, the friction factor, and the thermal performance.

Acknowledgements—This research was supported by the National Science Foundation (Grant No. CTS-8910860).

REFERENCES

1. F. Burggraf, Experimental heat transfer and pressure drop with two-dimensional turbulence promoter applied to two opposite walls of a square tube. In *Augmentation of Convective Heat and Mass Transfer* (Edited by A. E. Bergles and R. L. Webb), pp. 70–79. ASME, New York (1970).
2. J. C. Han, Heat transfer and friction in channels with two opposite rib-roughened walls, *ASME J. Heat Transfer* **106,** 774–781 (1984).
3. J. C. Han, J. S. Park and C. K. Lei, Heat transfer enhancement in channels with turbulence promoters, *ASME J. Engng Gas Turbines Pwr* **107,** 629–635 (1985).
4. S. C. Lau, R. D. McMillin and J. C. Han, *Turbulent Heat Transfer and Friction in a Square Channel with Discrete Rib Turbulators*, ASME HTD-Vol. 120, pp. 33–41 (1989), and *ASME J. Turbomachinery*, in press.
5. S. C. Lau, R. D. McMillin and J. C. Han, Heat transfer characteristics of turbulent flow in a square channel with angled discrete ribs, ASME Paper No. 90-GT-254 (1990), and *ASME J. Turbomachinery*, in press.
6. S. J. Kline and F. A. McClintock, Describing uncertainties in single-sample experiments, *Mech. Engng* **75,** 3–8 (1953).

EFFETS DES ARRANGEMENTS DE NERVURES EN V SUR LE TRANSFERT THERMIQUE TURBULENT ET LE FROTTEMENT POUR UN ECOULEMENT ETABLI DANS UN CANAL CARRE

Résumé—On examine le transfert thermique et le frottement pour un écoulement établi d'air dans un canal carré ayant deux parois opposées rugueuses avec des arrangements alignés de nervures en V. La rugosité par nervures modélise les passages de refroidissement interne dans les ailettes de turbines à gaz modernes. Les angles d'attaque des arrangements de nervures en V sont 45°, 60°, 90°, 120° et 135°. Les nervures avec 60° et $p/e = 10$ ont le transfert le plus élevé pour un débit d'air donné et le plus fort transfert de chaleur par unité de puissance de pompage. Elles sont recommandées pour le refroidissement d'ailettes de turbine en remplacement des nervures pleines à 45° et 60°.

EINFLUSS EINER V-FÖRMIGEN BERIPPUNG AUF WÄRMEÜBERGANG UND DRUCKABFALL IN EINER VOLLSTÄNDIG ENTWICKELTEN TURBULENTEN STRÖMUNG IN EINEM QUADRATISCHEN KANAL

Zusammenfassung—Die vorliegende Arbeit befaßt sich mit dem Wärmeübergang und dem Druckabfall in einer vollständig entwickelten turbulenten Luftströmung in einem quadratischen Kanal, in welchem zwei gegenüberliegende Wände mit Anordnungen aus V-förmigen Rippen künstlich aufgerauht sind. Dieser künstlich aufgerauhte Kanal ist als Modell für die Kühlkanäle in der Beschaufelung moderner Gasturbinen vorgesehen. Der Anstellwinkel der V-förmigen Rippenanordnung beträgt 45, 60, 90 (wie bei Vollrippen), 120 und 135 Grad. Die V-förmigen Rippen bei 60 Grad und $p/e = 10$ rufen bei gegebenem Luftdurchsatz den höchsten Wärmeübergang für berippte wie auch für glatte Wand hervor. Es ergibt sich auch der höchste Wärmeübergang für den gesamten Kanal bei gegebener Gebläseleistung. Diese Anordnung wird daher für die innere Kühlung von Turbinenschaufeln vorgeschlagen—sie soll die Vollrippen mit 45 Grad oder 60 Grad ersetzen.

ВЛИЯНИЕ ОРЕБРЕНИЯ С V-ОБРАЗНОЙ ФОРМОЙ РЕБЕР НА ТУРБУЛЕНТНЫЙ ТЕПЛОПЕРЕНОС И ТРЕНИЕ ПРИ ПОЛНОСТЬЮ РАЗВИТОМ ТЕЧЕНИИ В КАНАЛЕ КВАДРАТНОГО СЕЧЕНИЯ

Аннотация—Исследуются характеристики турбулентного теплопереноса и трения при полностью развитом течении воздуха в канале квадратного сечения с шероховатостью двух противоположных стенок, образованной упорядоченными рядами ребер V-образной формы. Течение в оребренном таким образом канале моделирует процессы охлаждения лопаток газотурбинных двигателей. Эксперименты проводились для углов атаки на V-образное ребро 45°, 60°, 90°, 120° и 135°. Показано, что максимальный коэффициент теплопереноса к оребренной и гладкой стенке, а также максимальный коэффициент теплообмена в канале на единицу подводимой мощности достигается при угле атаки 60° и отношении $p/e = 10$.